Peer reviewed version

Link to published version (if available):
10.1088/1748-0221/14/08/P08005

Link to publication record in Explore Bristol Research
PDF-document

University of Bristol - Explore Bristol Research
General rights

High-resolution imaging of nuclear waste containers with Muon Scattering Tomography

View the article online for updates and enhancements.

IOP ebooks™

Bringing you innovative digital publishing with leading voices to create your essential collection of books in STEM research.

Start exploring the collection - download the first chapter of every title for free.

High-resolution imaging of nuclear waste containers with Muon Scattering Tomography

L. Frazão,[a] **J.J. Velthuis,**[a,b,c,1] **S. Maddrell-Mander**[a] **and C. Thomay**[a]

[a]*H.H. Wills Physics Laboratory, University of Bristol,*
Tyndall Avenue, Bristol, U.K.

[b]*Swansea University, Medical School,*
Singleton Park, Swansea, U.K.

[c]*School of Nuclear Science and Technology, University of South China,*
No 28 West Changsheng Rd, Hengyang, China

E-mail: jaap.velthuis@bris.ac.uk

Abstract: A method was developed to determine the edge position of uranium blocks embedded in concrete, using Muon Scattering Tomography. This method is useful for nuclear waste management, as it provides a precise image of high-Z materials inside nuclear waste drums. Simulations were performed of uranium blocks with different sizes, encased in a concrete tube, and their lengths were reconstructed. The resolution obtained for the reconstructed lengths was 2.9 ± 0.5 mm and the method works down to a smallest size of 5 mm. This result was obtained without including the muon momentum. The same method was then applied including the momentum information, resulting in a better resolution of 0.96 ± 0.03 mm, and works down to a smallest size of 2 mm.

---

[1]Corresponding author.

Contents

1 Introduction

Developing techniques to scan nuclear waste, imaging and finding materials without having to open their containers is essential for the management of legacy nuclear waste. Knowing the position and size of high-Z materials inside nuclear waste vessels can help to determine the presence and respective amount of special nuclear materials. This information can then be used to decide the appropriate way of disposal of nuclear waste.

Muon scattering tomography (MST) is a technique that uses the muons that are naturally produced in the atmosphere by cosmic rays as scanning probes [1]. Muons are highly penetrating particles, which makes them a good candidate to study dense materials, since most of them will cross large amounts of such materials without being absorbed. They are an ubiquitous and free source, which does not introduce additional radiation in the volume to be scanned, and that can be used over large areas.

Because they are charged, muons undergo multiple Coulomb scattering [2–4]. The width of the distribution of their projected scatter angles (σ) is given by

$$\sigma \approx \frac{13.6 \text{ MeV}}{\beta c p} z \sqrt{X/X_0}(1 + 0.038 \ln(X/X_0)) \tag{1.1}$$

where p is the momentum of the muon, βc its velocity, z its charge number, X the thickness of the material, and X_0 the radiation length [4] which is given by

$$X_0 \approx \frac{A \cdot 716.4 \text{ g/cm}^2}{\rho \cdot Z(Z+1) \ln\left(287/\sqrt{Z}\right)} \tag{1.2}$$

where A is the mass number, Z the atomic number and ρ the density of the material traversed. Hence the width is higher for higher atomic number Z of the material crossed. Thus by measuring the width of the scattering angle distribution information on the crossed material can be extracted. The scattering angle for a single muon can be measured by tracking the muon before and after crossing the volume.

Several methods were developed to perform imaging of high-Z materials embedded in concrete, such as [5] and [6], which are also based on scattering density in voxels, and were applied by other groups, such as in [7, 8] and [9]. We have developed our own method for imaging volumes of high-Z materials in concrete [10], which achieved a resolution of 1.2±0.5 mm but used the momentum information. Here we present a much improved version of the algorithm. A description of the original algorithm and the improvement is given in section 3. One of the improvements is that the improved algorithm can also be applied without momentum information, albeit resulting in a worse resolution. This is important as it is not possible to measure the muon momentum with our current set up without an error on the order of 30-200%.

2 Methods

Our previous method exploited the fact that, since the width of the scattering angle distribution is larger for high-Z materials compared to concrete, the concentration of vertices with tracks with large scattering in a voxel is higher (see section 3 and [10]). Hence, moving the voxel grid our discriminating variable will change when moving between high-Z material and concrete. Our new method uses a multivariate analysis. The algorithm was developed and tested using a Monte Carlo simulation based on the performance of our small demonstrator system.

2.1 Simulations

Simulations were performed in Geant4 [11, 12] version 9.4, including the muon processes of multiple scattering, ionisation, Bremsstrahlung and pair production. An illustration of the simulation setup is shown in figure 1. The sample to be measured was a concrete cylinder of 13 cm radius and 40 cm length, inside a 1.5 mm thick steel container. The size of this sample was chosen to be the same as a mock waste drum we previously tested with the detector system. A rectangular cuboid uranium block was placed inside the concrete. This shape for the uranium block was chosen for simplicity. The uranium block was simulated with different sizes in the x direction (along the length of the cylinder); blocks where this length was above 30 mm were cubic, and blocks with less than 30 mm in x were 30 mm long in y and z.

Both above and below the sample there were 3 layers of detector pairs (to measure the x and y position of the muon), with an area of 1×1 m^2. These were simulated as resistive plate chambers (RPCs) [13]. The RPCs were 6 mm thick, and made of glass. The spacing between each xy pair was 19 mm, and 58 mm between each of the pairs. The height between the upper and lower tracking systems was 548 mm. The drum was placed in the centre of this space, which means that there were 274 mm between the centre of the drum and both the upper and lower plates closest to the drum. The detector resolution was 450 μm and the angular resolution was 2.75 mrad. All performance parameters like the hit resolution are the same as measured with our small prototype system [13].
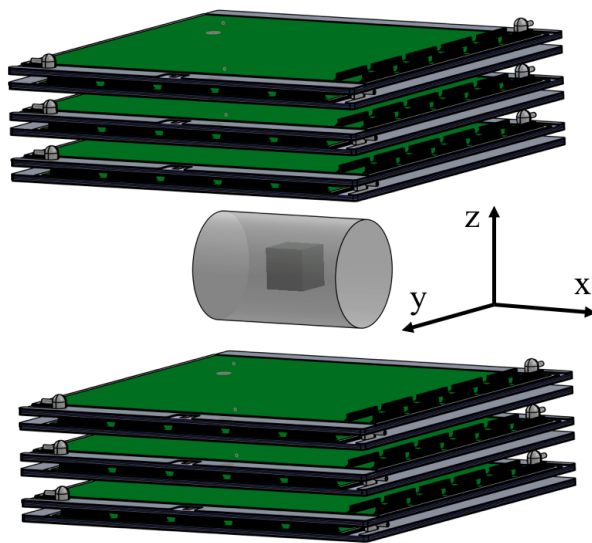
Figure 1. Illustration of the simulation geometry.

The cosmic-ray muons were simulated with CRY [14], which provides angle and momentum distributions of cosmic rays. For each uranium block size, 5 simulations were performed, using the number of muons corresponding to 500000 seconds (139h, or about 5.8 days), with 7000 muons per m^2 per minute. With this rate, the total data taking time for the 5 simulations corresponds to 29 days.

2.2 Simulation validation

In order to validate the simulation, data was taken with our prototype detector system [13] which used 50×50 cm^2 RPCs. The prototype system was built to provide experimental data for a study into the detection of lumps of high-Z materials in cargo containers [15, 16]. These lumps are detected using the metric distance distribution of scattering vertices. This variable is explained in more detail in section 3.[1] Figure 2 shows the discriminator distribution, which is the median of the metric distance, obtained in real data [17] and figure 3 shows the same distribution using our simulation framework [17]. The distributions were obtained from scanning a $10 \times 10 \times 15$ cm^3 lead block. A χ^2 test comparing the two distributions was performed, resulting in a p-value of 0.8, demonstrating a good correspondence between experimental data and simulation.

2.3 Track fitting

The muons generated by CRY were propagated through the set-up and the hit positions were smeared with the measured position resolution. The output from Geant4 of the hit positions on the detector plates was analysed with a ROOT [18] application that performed a fit of the upper and lower tracks, as described in [15]. For a system with 3 pairs (for *x* and *y* directions) of upper and 3 of lower detector layers, 12 hit points are obtained for each muon. A first fit is performed separately for

---

[1]This metric distance was weighted by the KNN (k-nearest neighbors) discriminator of both tracks [17] instead of the angle and momentum which is used in the current paper.
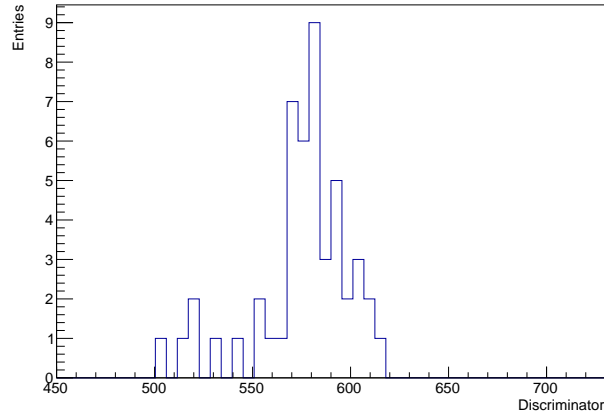
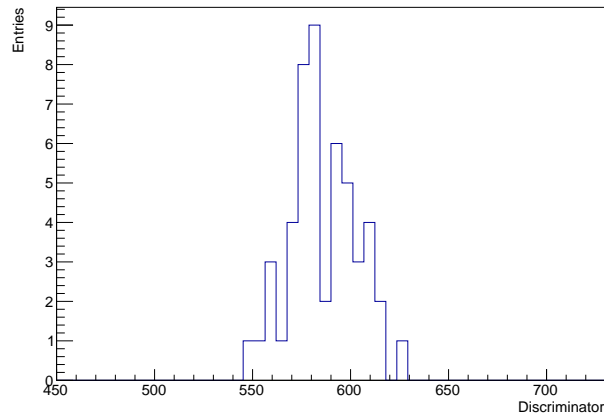**Figure 2**. Discriminator value for experimental data, from a $10 \times 10 \times 15$ cm^3 lead block.

Figure 3. Discriminator value for simulation, from a $10 \times 10 \times 15$ cm^3 lead block.

each 3 points in upper and lower, x and y directions, to guarantee that a good muon track is found. Subsequently, in a second step, all the 12 points obtained from an event are fitted at the same time, demanding an incoming and outgoing track meeting in a vertex. The fit has 7 parameters, which are the 4 track slopes (for upper and lower, x and y) and the 3 coordinates of the vertex position. This is done by minimising, using MINUIT [19], the function

$$E = E_x + E_y. \tag{2.1}$$

E_x (and, analogously, E_y) is given by

$$
E_x = \sum_{i=1}^{3} \frac{(h_i - (v_x + k_{x,\text{upper}} \cdot (z_i - v_z)))^2}{\sigma_{h_i}^2}
$$
$$
+ \sum_{i=4}^{6} \frac{(h_i - (v_x + k_{x,\text{lower}} \cdot (z_i - v_z)))^2}{\sigma_{h_i}^2} \tag{2.2}
$$

where h_i are the measured hit positions, z_i the vertical position of the detectors, v_x, v_y, v_z the vertex positions, k the track slopes, and σ_{h_i} the errors on the measurement of the hit positions. Figure 4 illustrates the track and vertex fit principle. It is a 2D representation for simplicity, but the fit is performed in 3D. The scatter vertex point calculated by the fit is not a real point where the muon scattered, since muons scatter in multiple points, but it is a useful approximation. The χ^2 values from the 3-point fits and from the combined fit are calculated and used as a cut: tracks with χ^2 values above the cut are discarded. This is an advantage of the vertex method over the other commonly used method of the point of closest approach. Tracks with a reconstructed vertex outside the volume of interest are also rejected. For accepted tracks and vertices, variables such as the scattering angle and offsets are calculated for further analysis. About 99% of the tracks pass these cuts.
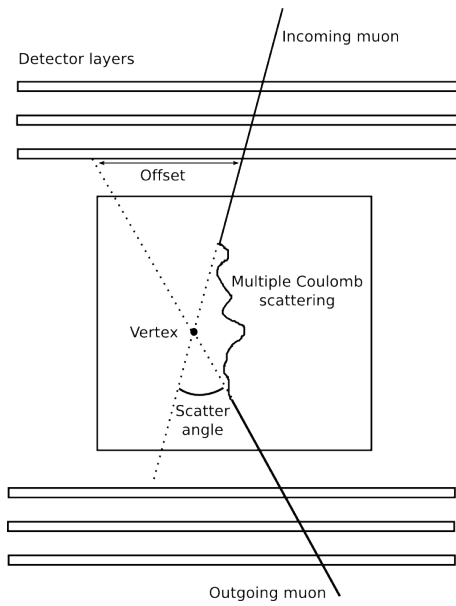

Figure 4. Illustration of the muon scattering principle and vertex reconstruction. The figure is shown in 2D for simplicity, but it should be noted that the measured angle is in 3D, although projected angles in 2D can also be calculated. The sizes are exaggerated in order to better visualise the difference between the multiple scattering and the reconstructed vertex.

3   Metric distance method

Our previous imaging method, described in [10], exploits the fact that the concentration of vertices with high scattering angles is large for high-Z materials. Therefore, it divides the volume of interest in cubic voxels with a side of 1 cm, takes a fixed number of tracks in each voxel with the highest scatter angle and calculates a weighted metric distance for each pair of tracks, as

$$m_{ij} = \frac{\left\|\vec{v}_i - \vec{v}_j\right\|}{(\theta_i p_i)(\theta_j p_j)}, \tag{3.1}$$

where $\vec{v}_i$ is the reconstructed vertex position of muon i, θ_i its scatter angle and $p_i = \frac{\hat{p}_i}{p_0}$, where $\hat{p}_i$ is its momentum (if it is available) and $p_0 = 3\,\mathrm{GeV}$ is a reference momentum. This algorithm was first

developed for homeland security applications, where the voxels used were larger, and it was only necessary to determine if a voxel contained a high-Z material, which would be identified by a high density of highly scattered muons [15]. For applications using small voxels, like imaging nuclear waste drums, the distribution of distances $\|\vec{v}_i - \vec{v}_j\|$ should be the same for all homogeneously filled voxels, therefore only the weighting by the angle and momentum will be relevant. However, the distribution of the distance between vertices of highly scattered angles will be relevant for non-homogeneously filled voxels, such at the edge of the blocks, making it a good method to identify edges [10]. The distributions of the metric distance are also sensitive to the presence of voids in the concrete [20].

In [10] the number of chosen tracks were the most scattered 26 in each voxel, whose combination in pairs gives a number of entries in each metric distance graph of 325. The distribution of the logarithm of the metric distance, $\ln(m_{ij}/m_0)$, was plotted for each voxel ($m_0 = 1$ m·rad^{-2} is a reference value so that the variable in the logarithm has no units). Figure 5 shows examples of two of those distributions; one for a voxel filled with concrete and one filled with uranium. When moving the grid inside the concrete object with the uranium inclusion distributions are obtained containing components due to uranium and to the concrete. These distributions were fitted with two Landau distributions, where the peak locations were fixed to the values for the metric distance obtained when only using concrete and uranium. For each voxel the ratio of the amplitude of two fitted Landaus for concrete and uranium was calculated. To obtain a good resolution determining the edges of the blocks, this was done for several grids, with the same voxel size but each shifted by 1 mm in the direction of the edge scanning (the x-axis, along the length of the concrete cylinder). When defining the start and finish of each block as the voxel where the amplitude fraction exceeded 99% for uranium, a resolution of 1.2±0.5 mm was obtained using simulated muon data equivalent to 25 days of data taking.

4 Edge finding method

The previous method works well, but it requires the true momentum information which is experimentally not available. In the new method [21], shown in this paper, the distributions of $\ln(m_{ij}/m_0)$ were fitted with a single Landau distribution convoluted with a Gaussian but the peak locations are left free. The same number of tracks (26) was used. This value was chosen as a balance between having enough tracks to see the distribution shape and perform the fit, and not taking too much time to perform the calculations. As the chosen tracks are the most scattered ones, increasing this number (for the same data taking time) adds tracks with a lower scattering angle, which give less information. An example of these distributions and fits can be seen in figure 5. There is no physics reason why the distributions follow a Landau convoluted with a Gaussian, but the fit describes most distributions well. To improve on the previous method we moved on to a multivariate analysis (MVA) method. This method was performed using the ROOT package TMVA [22]. The MVA method used was the Fisher linear discriminant [23], which is a supervised method (the training data includes label information on the respective class) that separates the data into two classes. In summary, this method finds the plane **w** in the L-dimensional space, for L variables measured, so that projected samples from the two classes onto **w** are better separated.

Here the Fisher linear discriminant was trained using simulations of muons going through either a solid concrete block or a solid uranium block. Variables from the fit, in particular the width, the peak position, and the peak amplitude, as well as variables from the histogram such as the maximum
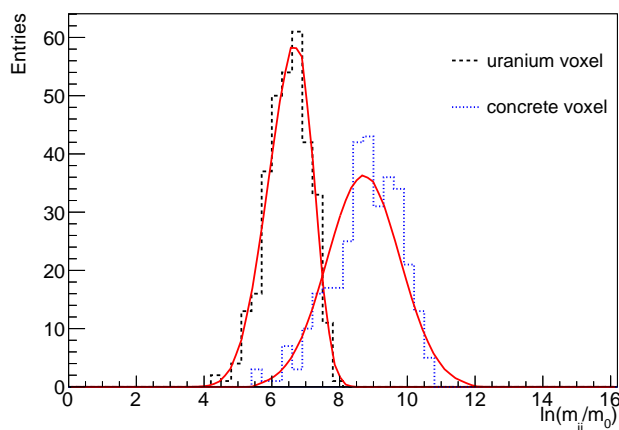
Figure 5. Distributions of the logarithm of the metric distance for a voxel inside uranium and a voxel in concrete, as well as respective fit with a Landau distribution convoluted with a Gaussian.

value and respective bin position, were fed into the Fisher algorithm as benchmark results. The training samples used were obtained from voxels with only concrete and only uranium (from uranium blocks of $4 \times 4 \times 4$ cm^3). For the training samples the probability that a voxel contained uranium was extracted. This probability can be seen in figure 6. As, in practice, the muon momentum is either not measured, or measured with a large uncertainty, the momentum was not used in these results. Section 6 will show results for an ideal system that measures the muon momentum.

Next, runs with blocks of uranium were simulated and the metric distance distribution for each voxel was fitted and the probability that the voxel was either uranium or concrete was calculated using the Fisher linear discriminant. As in the previous method, this was done for several voxel grids, shifted by 1 mm. Figure 7 and 8 show examples of the Fisher probability output ξ as a function of different voxel edge locations for a 1 cm and a 4 cm block respectively. Each point in these figures is the average of the values from the 5 simulations with the same block size for single voxels along x, at fixed y and z values. The Fisher probability does not reach 1 for all the values of x in the uranium region, but it is still easy to distinguish the uranium from the much lower concrete background, and consequently reconstruct the block length. The Fisher probability in the concrete background is zero, barring a few unphysical spikes which can be filtered out easily, since real uranium pieces will give non-zero values for several adjacent voxel locations. For the case without momentum, the block lengths were measured by taking the region between the first and the last point whose ξ was above a threshold of 0.1. Uncertainties on the measurement of the length of each block were calculated by performing the same length measurement for 5 different simulations with data corresponding to 5.8 days of muon flux each, and calculating the standard error on the mean.

As the reconstructed vertex is not a real scattering vertex but just a useful assumption, tracks scattered with large scattering angles in the uranium can give rise to reconstructed vertices in the concrete and vice-versa. This leads to a phenomenon we refer to as mixing. Voxels close to the edge of the material will contain vertices that actually belong to the other material. This does not occur far away from the edge. This mixing range extends for approximately 5 mm with the given geometry of this study. It is this mixing range that determines the performance of the resolution algorithm.

If the block is bigger than the mixing range, the edge resolution will be the same irrespective of the actual size of the block. If the block is smaller than the mixing range, then there is no longer contrast between the two materials and thus it becomes impossible to find the edge of the block. As such, it was not possible to measure lengths smaller than 0.5 cm. As an example of the Fisher probability output obtained for these small blocks, figure 9 shows an example of a 0.3 cm block, where it is impossible to distinguish the uranium from the concrete background.
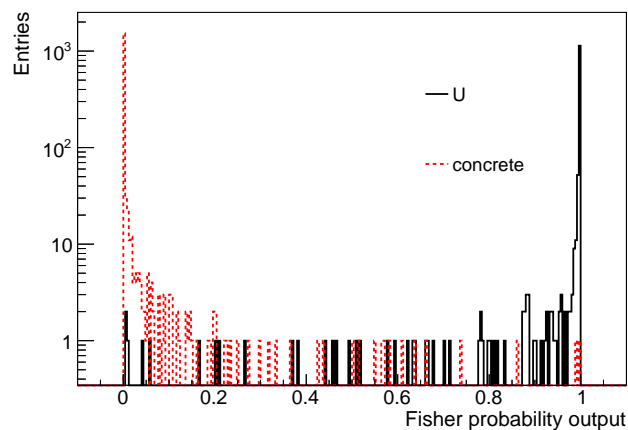
Figure 6. Output from the training with the Fisher linear discriminant, using samples of pure concrete and pure uranium.
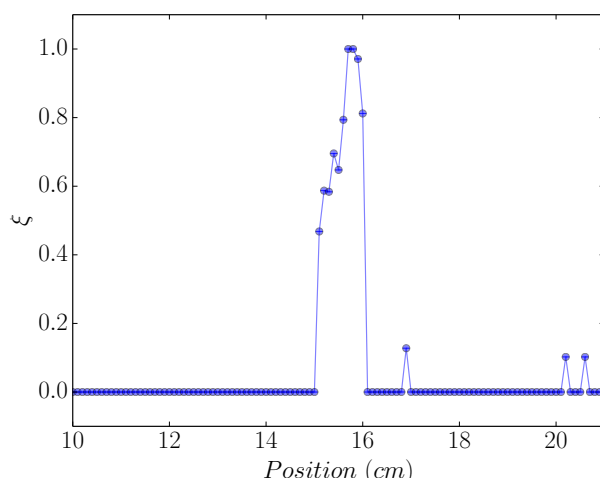

Figure 7. Fisher probability output, ξ, as a function of the x coordinate for a 1 cm block of uranium inside concrete, before calibration.
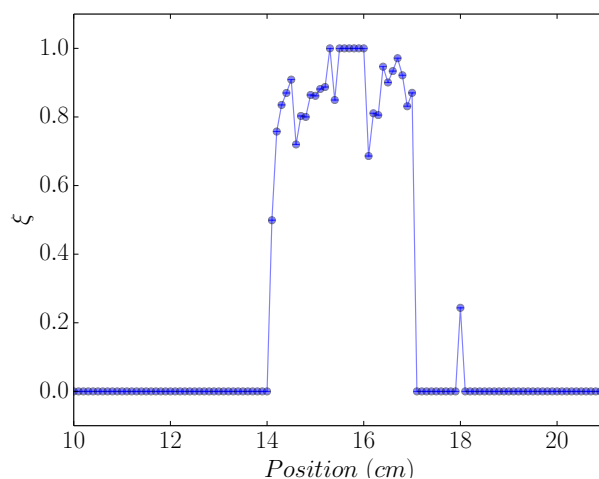
Figure 8. Fisher probability output, ξ, as a function of the x coordinate for a 4 cm block of uranium inside concrete, before calibration.
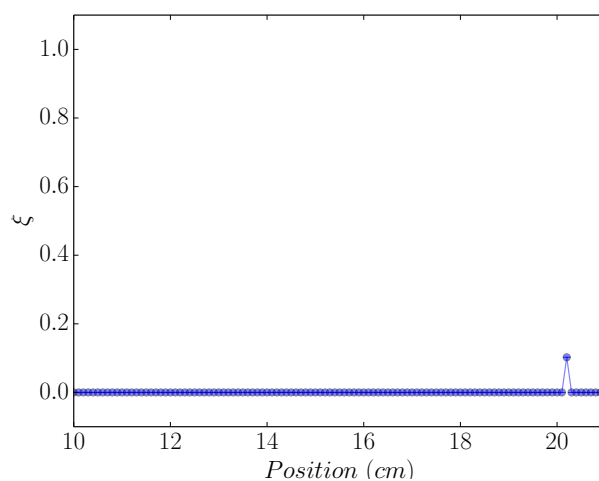

Figure 9. Fisher probability output, ξ, as a function of the x coordinate for a 0.3 cm block of uranium inside concrete.

5 Results

Several uranium blocks were simulated, with sizes varying from 0.5 cm to 5 cm. Figure 10 shows the reconstructed sizes as a function of the simulated sizes. The reconstruction was repeated 5 times for each size. The error bars represented the standard error on the mean for each generated size. The variation in the size of the error bars is due to the limited amount of repeats. A clear linear relationship between the reconstructed and the generated sizes is observed, as

$$\text{Reconstructed Size} = (0.65 \pm 0.03) \times \text{Real Size} + (0.34 \pm 0.08) \text{ cm}. \tag{5.1}$$

The slope and intercept are due to the fixed size of the 1 cm voxels, and to the "mixing region" around the uranium blocks, where some vertices of muons that scattered in uranium are reconstructed in concrete and vice-versa: for blocks that are close to the voxel size or smaller, most voxels from the 1 mm shifts contain the mixing regions from both sides of the block, stretching their measured length, while for larger blocks the voxels at each edge only contain the mixing region of the respective edge. Therefore, it was necessary to calibrate the reconstructed lengths. Each point was calibrated by performing the fit excluding that point and using the resulting equation to obtain the corresponding calibrated length. These fits were performed using a χ^2 fit. The calibrated reconstruction results are shown in figure 11. The fit line performed after the calibration yields

$$\text{Reconstructed Size} = (1.01 \pm 0.05) \times \text{Real Size} - (0.01 \pm 0.13) \text{ cm}. \tag{5.2}$$

Hence, the calibrated reconstructed size and the real size are the same within errors. The uncertainty in the reconstructed length is independent on the real size for blocks larger than the mixing region of about 5 mm. This can be seen from the size of the error bars. Because of this and since the reconstructed size is linearly dependent on the real size, we can combine all data points in this graph to calculate the position resolution as the standard deviation of the reconstructed minus the real size, as

$$\sigma = \sqrt{\frac{\sum_i (l_{t,i} - l_{r,i})^2}{n}}, \tag{5.3}$$

where $l_{t,i}$ is the true simulated size, $l_{r,i}$ the reconstructed sizes, and n the number of data points used. The resolution obtained was $\sigma = 2.9 \pm 0.5$ mm. With this technique it was possible to reconstruct the size of uranium blocks down to 0.5 cm. For smaller sizes, most points in the uranium region had Fisher probability values similar to concrete due to the mixing, making it impossible to perform this measurement. This is within errors the same as in our previously published result. However, the previously published result used the true momentum information. As such, this method is a significant improvement and represents a more realistic performance estimate.
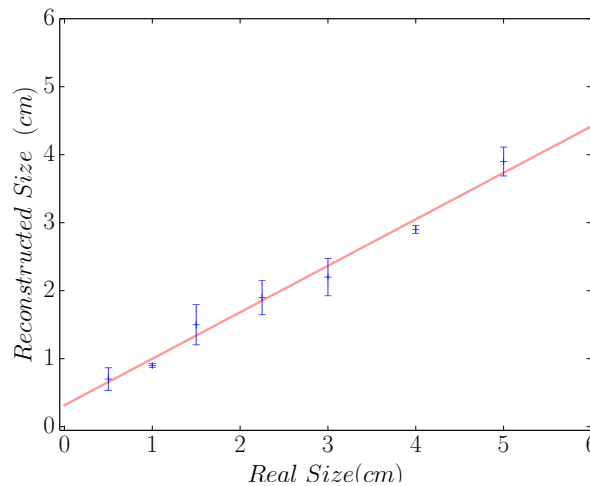

Figure 10. Reconstructed lengths against real lengths before calibration, including the linear function fitted to the data.
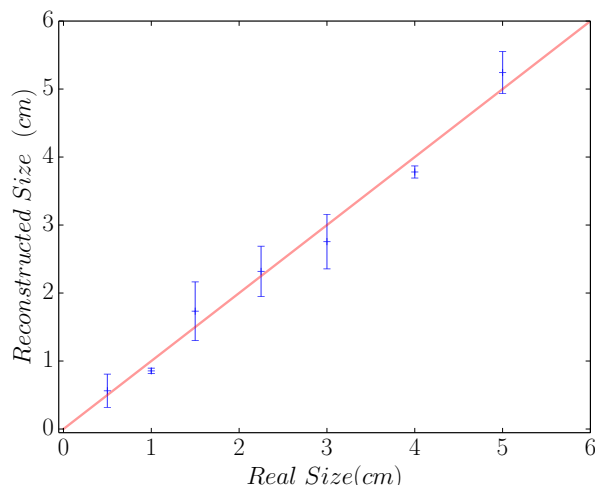
Figure 11. Reconstructed lengths against real lengths, after calibration.

6 Results using momentum information

This study was also performed using the momentum information, in order to show how this information would improve the method for an ideal muon tomography system that could measure the muon momentum with great precision and to demonstrate the significant improvement due to the use of the Fisher linear discriminant over the previous method that also used the true momentum information but a different analysis technique. The training for the MVA was also done using momentum since this changes the distribution of the metric distance. Using the momentum leads to a smaller mixing region as tracks with large scattering angles yielding uranium-like vertices in concrete are typically tracks with a very low momentum (see equation (1.1)). By adding the momentum information, these tracks no longer bias the metric distance towards uranium. Figure 12 shows the metric distance distributions for a uranium voxel and a concrete voxel (equivalent to figure 5, but using momentum information), achieving a better peak separation that the case without momentum. Figure 13 shows the Fisher probability output from the training data with pure concrete and pure uranium voxels. The training in this case was performed using voxels from the edges of a uranium block of $18 \times 18 \times 18$ cm^3. This accounts for the different results from the training than the ones obtained without momentum (figure 6). Figure 14 and 15 show examples of this reconstruction for a 3 cm and a 0.5 cm block respectively. In this case, the threshold on the ξ discriminant to determine the edges of the blocks was chosen to be 0.9. The differences in the fluctuations of the concrete between with and without momentum information are most likely due to the differences in the training for both cases.

The method was applied to measure the length of several blocks of uranium with different sizes, from 0.2 cm to 10 cm, embedded in concrete. The reconstructed sizes versus the real sizes are shown in figure 16, and the respective linear fit yields

$$\text{Reconstructed Size} = (0.76 \pm 0.01) \times \text{Real Size} + (0.44 \pm 0.02) \text{ cm}. \tag{6.1}$$

This fit result is used to calibrate the reconstructed sizes. These results can be seen in figure 17.
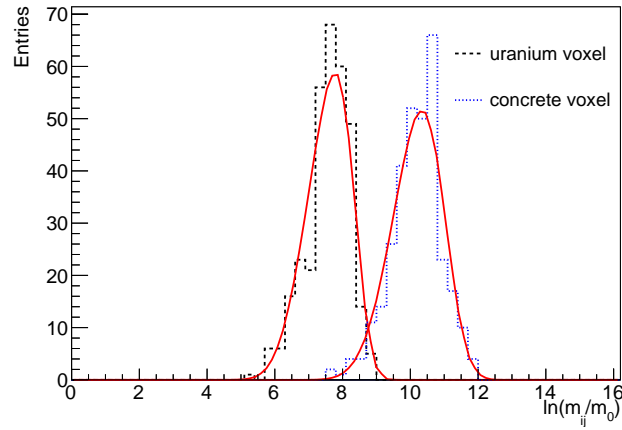
Figure 12. Distributions of the logarithm of the metric distance for a voxel inside uranium and a voxel in concrete, as well as respective fit with a Landau distribution convoluted with a Gaussian, using momentum information.
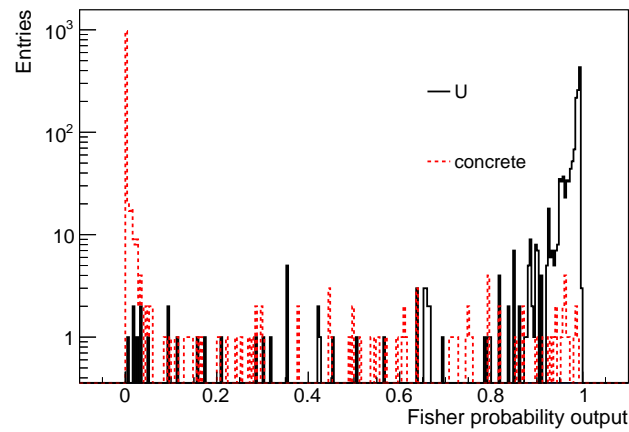

Figure 13. Output from the training with the Fisher linear discriminant, using samples of pure concrete and pure uranium, using momentum information.

The straight line fit for the edge reconstruction using momentum information yielded

$$\text{Reconstructed Size} = (0.99 \pm 0.01) \times \text{Real Size} - (0.01 \pm 0.03) \text{ cm,} \qquad (6.2)$$

so the slope and intercept are compatible within errors to 1 and 0 respectively.

The resolution obtained was $\sigma = 0.96 \pm 0.03$ mm, showing a significant improvement over the previous result of 1.2±0.5 mm [10]. For lengths lower than 0.2 cm, it was not possible to measure the uranium block, because the points corresponding to the uranium in the Fisher probability graphs were similar to the ones from the concrete background, due to the size of the mixing region.
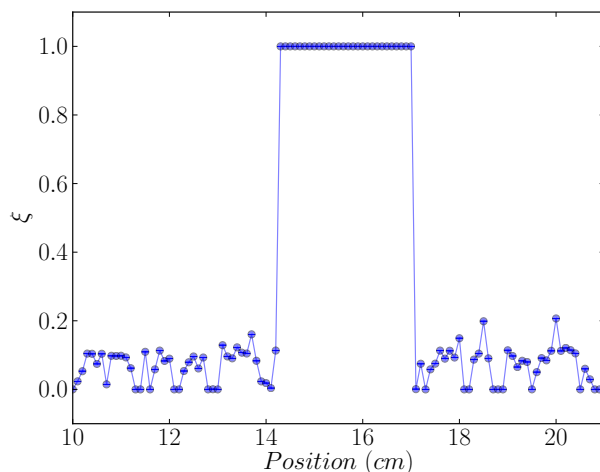
Figure 14. Fisher probability output, ξ, as a function of the x coordinate for a 3 cm block of uranium inside concrete before calibration, using momentum information.
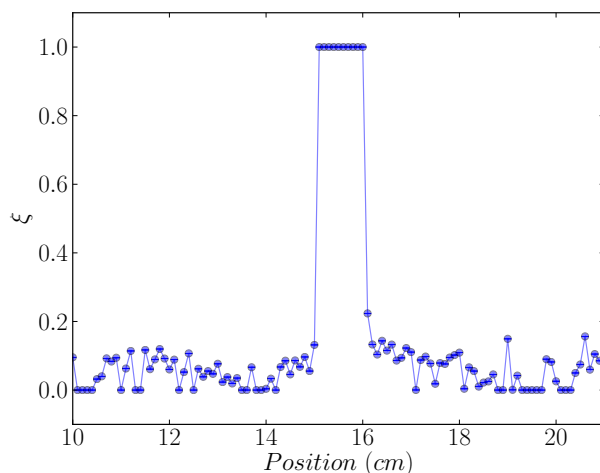

Figure 15. Fisher probability output, ξ, as a function of the x coordinate for a 0.5 cm block of uranium inside concrete before calibration, using momentum information.

7 Conclusions

Muon tomography can be used to scan nuclear waste containers. Previous results have shown that it is possible to find high-Z material lumps in concrete and determine edges of uranium blocks embedded in concrete. Here we have shown, using our validated Monte Carlo simulation, the proof of principle of a method, focusing on measuring uranium blocks, that is a significant improvement on our previously published results. A resolution of $\sigma = 2.9 \pm 0.5$ mm measuring lengths of simulated uranium blocks between 0.5 cm and 5 cm was obtained. For blocks smaller than 5 mm, there is not sufficient contrast in the metric distance distributions between the voxels in the concrete and in the uranium. This method did not use momentum information, since preliminary studies to measure the
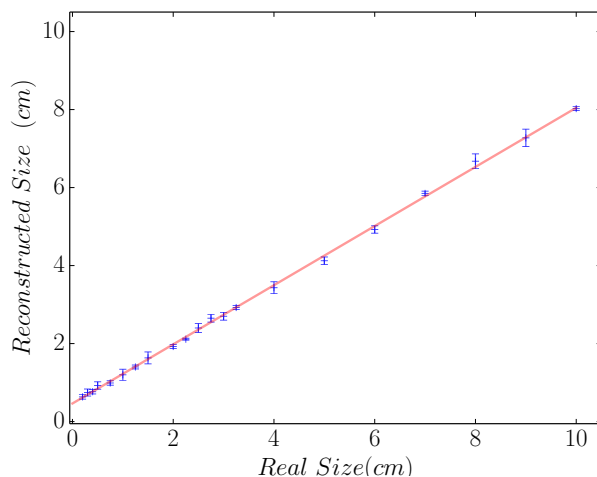
Figure 16. Reconstructed lengths against real lengths before calibration, including the linear function fitted to the data (Equation 6.1), using momentum information.
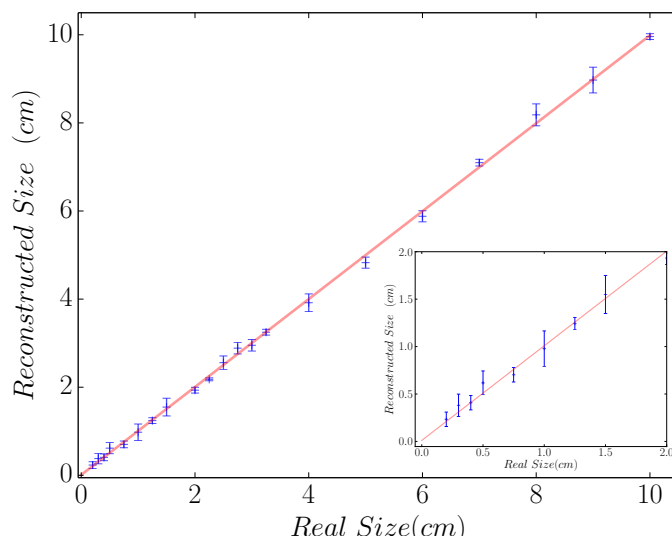

Figure 17. Reconstructed length against real length, after calibration, using momentum information. The inset is the same graph zoomed in the lengths under 2 cm.

momentum with a muon tomography system using multiple scattering in the detector planes show momentum resolutions between 30% and 200%. To make a fair comparison to our previous published result and to find out how much the use of the Fisher linear discriminant improved the result, the study was also done using the momentum information. It was shown that using the momentum information provides a better edge definition, with a resolution of $\sigma = 0.96 \pm 0.03$ mm, for lengths between 0.2 cm and 10 cm. It was not possible to measure lengths smaller than 2 mm using momentum information. This is a major improvement on the 1.2 ± 0.5 mm obtained with the previous method.

Acknowledgments

References

[1] K.N. Borozdin et al., *Radiographic imaging with cosmic-ray muons*, *Nature* **422** (2003) 277.

[2] V.L. Highland, *Some practical remarks on multiple scattering*, *Nucl. Instrum. Meth.* **129** (1975) 497.

[3] G.R. Lynch and O.I. Dahl, *Approximations to multiple Coulomb scattering*, *Nucl. Instrum. Meth.* **B 58** (1991) 6.

[4] PARTICLE DATA GROUP collaboration, *Review of particle physics*, *Chin. Phys.* **C 38** (2014) 090001.

[5] L.J. Schultz et al., *Image reconstruction and material Z discrimination via cosmic ray muon radiography*, *Nucl. Instrum. Meth.* **A 519** (2004) 687.

[6] L. Schultz et al., *Statistical reconstruction for cosmic ray muon tomography*, *IEEE Trans. Image Processing* **16** (2007) 1985.

[7] S. Pesente et al., *First results on material identification and imaging with a large-volume muon tomography prototype*, *Nucl. Instrum. Meth.* **A 604** (2009) 738.

[8] G. Jonkmans, V. Anghel, C. Jewett and M. Thompson, *Nuclear waste imaging and spent fuel verification by muon tomography*, *Annals Nucl. Ener.* **53** (2013) 267.

[9] A. Clarkson et al., *Characterising encapsulated nuclear waste using cosmic-ray muon tomography*, 2015 *JINST* **10** P03020 [arXiv:1410.7192].

[10] C. Thomay et al., *Passive 3d imaging of nuclear waste containers with muon scattering tomography*, 2016 *JINST* **11** P03008.

[11] GEANT4 collaboration, *GEANT4: a simulation toolkit*, *Nucl. Instrum. Meth.* **A 506** (2003) 250.

[12] J. Allison et al., *GEANT4 developments and applications*, *IEEE Trans. Nucl. Sci.* **53** (2006) 270.

[13] P. Baesso, D. Cussans, C. Thomay and J. Velthuis, *Toward a RPC-based muon tomography system for cargo containers*, 2014 *JINST* **9** C10041.

[14] C. Hagmann, D. Lange and D. Wright, *Cosmic-ray shower generator (CRY) for Monte Carlo transport codes*, *IEEE Nucl. Sci. Symp. Conf. Rec.* **2** (2007) 1143.

[15] C. Thomay et al., *A binned clustering algorithm to detect high-Z material using cosmic muons*, 2013 *JINST* **8** P10013.

[16] C. Thomay et al., *A novel Markov random field-based clustering algorithm to detect high-Z objects with cosmic rays*, *IEEE Trans. Nucl. Sci.* **62** (2015) 1837.

[17] C. Thomay et al., *A novel technique to detect special nuclear material using cosmic rays*, *IEEE Nucl. Sci. Symp. Med. Imag. Conf. Rec.* (2012) 662.

[18] R. Brun and F. Rademakers, *ROOT: an object oriented data analysis framework*, *Nucl. Instrum. Meth.* **A 389** (1997) 81.

[19] F. James and M. Roos, *Minuit: a system for function minimization and analysis of the parameter errors and correlations*, *Comput. Phys. Commun.* **10** (1975) 343.

[20] M. Dobrowolska, J. Velthuis, L. Frazão and D. Kikoła, *A novel technique for finding gas bubbles in the nuclear waste containers using muon scattering tomography*, 2018 *JINST* **13** P05015.

[21] L. Frazão, *Imaging and material identification of nuclear waste with muon scattering tomography*, Ph.D. thesis, School of Physics, Faculty of Science, University of Bristol, Bristol, U.K. (2018).

[22] P. Speckmayer, A. Höcker, J. Stelzer and H. Voss, *The toolkit for multivariate data analysis, TMVA* 4, *J. Phys. Conf. Ser.* **219** (2010) 032057.

[23] R.A. Fisher, *The use of multiple measurements in taxonomic problems*, *Ann. Eugenics* **7** (1936) 179.